Comparative analysis of mechanical properties and energy absorption capabilities of functionally graded and non-graded thermoplastic sheet gyroid structures

Graded and non-graded sheet gyroid structures

Ramon Miralbes [a]*, Saul Higuera[b], David. Ranz[b], Jose Antonior Gomez[b]

[a]*Department of Design and Manufacturing, University of Zaragoza, Zaragoza, Spain, DIDYF, C/ María de Luna nº 4, 50018, Zaragoza, Spain, miralbes@unizar.es, +34/876765069*

[b]*Department of Design and Manufacturing, University of Zaragoza, Zaragoza, Spain, DIDYF, C/ María de Luna nº 4, 50018, Zaragoza, Spain, w.saulhiguera@gmail.com, +34/876765069*

[c]*Department of Design and Manufacturing, University of Zaragoza, Zaragoza, Spain, DIDYF, C/ María de Luna nº 4, 50018, Zaragoza, Spain, dranz@unizar.es, +34/876765069*

[d]*Department of Design and Manufacturing, University of Zaragoza, Zaragoza, Spain, DIDYF, C/ María de Luna nº 4, 50018, Zaragoza, Spain, jogomez@unizar.es, +34/876765069*

Keywords: Periodic cellular lattice structures, triply periodic minimal surfaces (TPMS), additive manufacturing, compression, energy absorption, thermoplastic

Comparative analysis of mechanical properties and energy absorption capabilities of functionally graded and non-graded thermoplastic sheet gyroid structures

Additive manufacturing allows the tailoring of the structure of energy-absorbing materials. It is thus feasible now to use light, printed structures instead of other materials such as foams and honeycombs, signifying greater possibilities for customization. Some of these structures are triply periodic minimal-surface structures that is a family of different structures like the gyroid one. Another benefit of additively manufactured graded structures, which foams or honeycombs lack, is the flexibility to vary the internal parameters along one or more directions. This study focuses on the comparative analysis of graded and non-graded gyroid structures for four common thermoplastic materials used in additive manufacturing. These structures are compared with each other under quasi-static compression testing, as well as with expanded polystyrene foam and solid samples of the thermoplastic materials. The analysis includes investigation of the stress–strain and specific stress–strain curves, capability of absorbing energy per unit weight and per unit volume, ideality, total efficiency, and normalized energy vs. normalized stress characteristics. We also analyze the internal fracture mechanism of the structures. The objective is to obtain more extensive knowledge of the behavior of non-graded structures.

Keywords: Periodic cellular lattice structures, triply periodic minimal surfaces (TPMS), additive manufacturing, compression, energy absorption, thermoplastic

1. Introduction

For the last fifty years, expanded polystyrene foams (EPS) have been the most common materials used to absorb energy in lightweight applications such as different types of helmets. Nevertheless, these materials have some drawbacks, such as a low resilience, which implies an inability to absorb multiple impacts [6,27], limitation on increasing the

specific energy absorption [11], low recyclability (especially in helmets that combine multiple materials), high thermal insulation [4], and limitation in producing foam with different stiffnesses. Some studies [14] have pointed out that owing to the various stiffnesses and vulnerabilities of different brain regions, it is essential to develop new helmets by tailoring material properties of the inner liner depending on the part of the head to be protected.

Advances in additive manufacturing (AM) could solve some of these problems because new geometries can be developed with different optimized energy-absorbing structures and configurations depending on the part of the head to be protected. In this way, triply periodic minimal-surface (TPMS) structures are identified to be extremely efficient solutions [31], [32], because they exhibit a minimal area in three coordinate directions, zero mean curvature free of straight lines and intersections, and low anisotropy [39]. Furthermore, strut-based structures have some angle limitations [25], require additional supports in the manufacturing process [40], and present stress concentration near the joint; TPMSs do not have these angle limitations or need these supports [42], [41] and exhibit a more uniform stress distribution [25], [35], [45], [1]. Note that TPMSs also present higher fatigue endurance [9], [36].

There are two main methods to generate TPMS solid gyroids; the first, which is being considered in this paper, results in a double or sheet-based gyroid that consists of two separate minimal surfaces with two different level sets of thickness *t* used as the external surfaces of the volume. The second method generates what is often referred to as strut, skeletal, or network gyroid by considering one of the subdomains divided by the surface as a solid. Other research works [19] [2] [37] have demonstrated that the double or sheet-based gyroid can exhibit superior mechanical properties to the skeletal latter.

Maskery et al. [24] [23] also studied the specific energy absorption (SEA) and observed that sheet gyroids have a three times higher SEA than that of skeletal gyroids. Other studies of gyroid structures [21] [10] [4] pointed out that these TPMS structures, for all densities, have the highest isotropy (with a Zener ratio constant with unity) compared with other TPMS structures (such as Schwarz P, Neovious, and diamond). Other woks [28] have compared the mechanical properties of different TPMS structures, which revealed the high specific mechanical properties of gyroid structures. In summary, it can be concluded that sheet-based gyroid TPMSs could be a promising substitutes for EPSs in terms of mechanical properties, manufacturing process, and structural stability, and thus, are the focus of this study.

Note that AM also facilitates the use of a range of materials with different structures and parameters, as well as the generation of solid zones. Therefore, the same material can be used for the main parts of the helmet, increasing recyclability. Contemporary helmets have an internal liner of EPS (that could be substituted by a TPMS structure), an outer shell of polycarbonate (which could be also substituted by a solid printed zone), and some elements made of acrylonitrile butadiene styrene (ABS) (which can also be generated using AM); thus, the different parts must be separated before the recycling process. Furthermore, AM enables the use of new materials for the internal liner, including some renewable origin materials such as polylactic acid (PA); however, these materials have relatively inferior mechanical properties. AM also allows for the generation of different TPMSs that can be modified depending on the part of the head that needs to be protected.

Finally, AM also allows varying of the TPMS variables, especially thickness, along a specific direction; the structures so formed are known as graded structures,

which can be customized to generate functionally graded materials (FGMs). FGMs have been used to optimize structures in some applications [22] such as orthopedic [20] and dentistry implants [29]. Maskery et al. [23] studied graded and non-graded Al-Si10-Mg trust lattice structures. In the graded structures, the relative density varied from 0.139 to 0.301 relative density (factor of variation of 2.16), generating an equivalent relative density of 0.22, which was compared with the 0.22 relative density for the non-graded structure. They observed that while non-graded structures followed the Gibson–Ashby model [15], graded structures presented a continuously increasing stress–strain curve and a layer-to-layer collapse. Additionally, the results show that graded structures can avoid non-desirable failures, such as diagonal shear bands, and cause a continuous increase of energy absorption and strengthening. Moreover, despite graded structures having lower maximum efficiency, the efficiency–strain diagram shows a more constant shape without peaks and valleys as in the case of non-graded structures. In the same way, the normalized energy absorption diagram has less variation.

The study by Gurminder et al. [34], of copper open cell, also reported the same conclusion related to the failure mechanism; they investigated a single type of graded structure by varying the thickness from 1 to 1.6 mm (factor of variation of 1.6). However, they reported that the material, although has a graded structure, follows the Gibson–Ashby model. Nevertheless, Maskery et al. [23] pointed out that there should be a factor of variation from which graded structures do not follow the Gibson–Ashby model.

Al-Saedi et al. [3] studied Al-12Si aluminum alloy strut-graded lattice structures with a variation of the relative density from 0.077 to 0.343 (factor of variation of 4.45), which was also compared with an equivalent non-graded structure with a relative

density of 0.185. The results of this study were similar to those obtained by Maskery et al. [23] regarding the failure mechanism and energy absorption rate.

However, concerning the modification of the variables of sheet gyroid structures, little is known about the effects on different polymeric materials or their behavior in energy absorption performance, especially when considering substitutes for current impact-absorption materials such as EPS.

In this study, we aim to investigate the different variables affecting the energy absorption performance of sheet gyroids for various fused deposition modeling (FDM) thermoplastics and two different factors of variation; finally, we compare their optimal configurations with those of EPS.

2. Materials and methods

2.1. Materials

The studied materials were Z-ULTRAT ABS, fused filament fabrication (FFF) Flexismart thermoplastic polyurethane (TPU), Fiberology polyamide 12 (PA12), and HR-870 polylactic acid (PLA) (Table 1). The specimens were generated by FFF with a 0.10-layer height using a Zortrax M200 3D printer; this machine was equipped with a 0.4 mm diameter nozzle. A 100% volume fraction cube of each material was also generated (Table 2) and tested as a comparison for the specimens in terms of properties with the same weight; additionally, to determine the mechanical properties of the fully dense solid material under tractions loads, some specimens have been generated and tested according with the ASTM D638 (table 1). The retraction distances, layer ventilation, and temperature were selected by considering the specifications of the material distributor and the 3D printer manufacturer for each material. Additionally, in

the case of PA12, to avoid hygroscopy, a desiccant box with a guided tube to the direct extruder was used.

Table 1. Main mechanical properties of the studied materials provided by the manufacturer.

	Manufacturer	**Tensile Strength (MPa) (σ_u)**	**Tensile Modulus (MPa) (E_0)**	**Flexural Modulus (MPa)**	**Elongation at break (%)**	**Density (kg/m^3)**
ABS	ZORTRAX ULTRA	29.8	1570.4	1080	11.08	1195
TPU	FFF Flexismart	28	21.2	n/a	600	960
PA12	Fiberology	48	1436.1	1200	n/a	1020
PLA	HR-870	32	2005.7	1979	n/a	1220

Table 2. Main mechanical properties of the materials of 100% volume fraction, under compression.

	Manufacturer	**Compression Elastic strenght (MPa)**	**Compression Young's modulus (MPa)**	**Density (kg/m^3)**
ABS	ZORTRAX ULTRA	69.18	1692.64	1195
TPU	FFF Flexismart	-	20.58	960
PA12	Fiberology	48.22	1491.91	1020
PLA	HR-870	68.79	1936.54	1220

An EPS foam with a density of 120 kg/m^3 (EPS120) was also studied, which is one of the most common materials for the interior energy absorption liner of motorcyclist helmets.

2.2. Methods

Materials were tested according to UNE-EN-ISO 844:2015 "Rigid cellular plastics - Determination of compression properties," so 50 mm cubic specimens were used and the specimens were tested under low strain rates (0.00166 s^{-1}) using an INSTRON 8032

uniaxial test machine equipped with a 100 kN load cell, which harnesses force and displacement to determine stress–strain curves.

A TPMS gyroid is represented by the level curvature equation of a gyroid (Eq. 1) defined by Shoen[33], where *a* is the unit cell size and *t* is the parameter that defines the wall thickness:

$$\mathrm{F(x,y,z)} = \sin\left(\frac{2\pi x}{a}\right)\cos\left(\frac{2\pi y}{a}\right) + \sin\left(\frac{2\pi y}{a}\right)\cos\left(\frac{2\pi z}{a}\right) + \sin\left(\frac{2\pi z}{a}\right)\cos\left(\frac{2\pi x}{a}\right) - t \quad (1)$$

Note that there is a close relationship between the volume fraction (ρ^*) and the parameter that defines the thickness, *t* [30]. Additionally, ρ^* is related to the density of the solid material (ρ_{solid}) and the measured density of the structure (ρ_{struct}):

$$\rho^* = \left(\frac{Volume_{struct}}{Volume_{solid}}\right) = \left(1 - \frac{\rho_{struct}}{\rho_{solid}}\right) \quad (2)$$

For graded gyroid structures, it is possible to control this parameter using a field that varies in any direction; herein, the linear variation with the *z*-direction has been studied, resulting in a continuously changing volume fraction. A period of 15 mm was selected for the 45 mm specimen, resulting in 3 cell units in each direction. A sufficiently low period length was selected to reduce the influence of the edge effect in the results, which is high enough to obtain a specimen that has adequate accuracy with the 3D model due to the resolution of the 3D printer.

Four different specimens were compared: two linear-graded structures with low and high variations of the volume fraction and two non-graded structures with equivalent volume fractions (Fig. 1). The four specimens were as follows:

- LG15%: Low-variation linear-graded gyroid structure having between a 10 and 20% volume fraction; the equivalent volume fraction was 15%, with a ratio of 2 between the lowest and highest volume fractions.

- NG15%: Non-graded gyroid structure with a 15% volume fraction.

- HG25%: High-variation linear-graded gyroid structure having between an 8.3 and 41.6% volume fraction; the equivalent volume fraction was 25%, with a ratio of 5 between the lowest and highest volume fractions.

- NG25%: Non-graded gyroid structure with a 25% volume fraction.

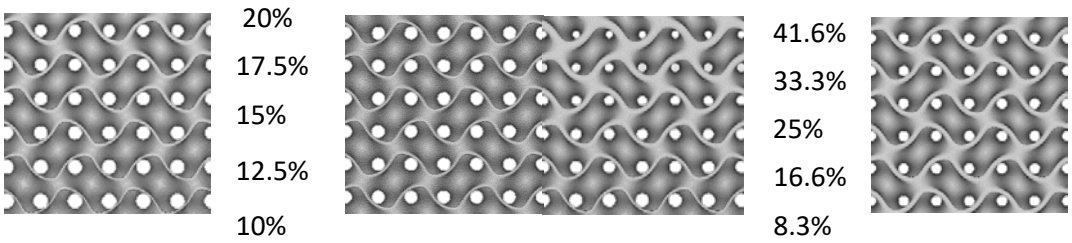

Figure 1. from left to right: LG15%, NG15%, HG25% and NG25% and the volume fraction in each zone

2.3 Interpretation of the results

Stress–strain curves are especially useful for obtaining the maximum mechanical property levels and the different points of the Gibson–Ashby model [15] (Fig. 2):

- Maximum specific compression strength in the elastic zone ($\sigma_{cs,e}$)

- Maximum specific compression strength at the densification point ($\sigma_{cs,d}$)

- Specific elastic Young's modulus (E_{cs})

- Specific plateau Young's modulus (E_{ps})

- Specific elastic absorbed energy (W_{es}):

$$\int_o^{\varepsilon_{c,d}} \sigma \, d\varepsilon \qquad (3)$$

- Specific energy absorbed in the plateau zone (W_{ps}):

$$\int_o^{\varepsilon_{c,p}} \sigma \, d\varepsilon \qquad (4)$$

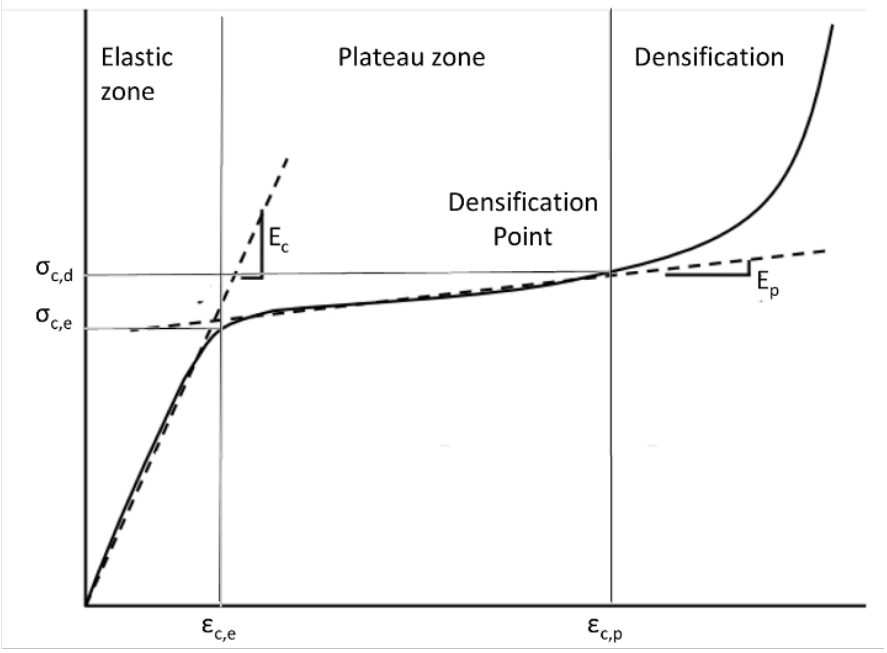

Figure 2. Stress–strain curve for a material that follows the Gibson–Ashby model.

In addition, the Gibson–Ashby model[15] also correlates the average stress in the plateau zone (σ_p), the elastic modulus (E_c) and the strain in the densification point ($\varepsilon_{c,p}$) with the relative density/ volume fraction and the main properties of the fully dense solid material under traction efforts: the Young's modulus (E_0) and the ultimate tensile strength (σ_u) through equations 5 to 7 where C_1, C_2 n_1, n_2 and α depens on the material, the load direction and the structure of the unit cell.

$$\frac{E_c}{E_0} = C_1 \cdot (\rho^*)^{n_1} \qquad (5)$$

$$\frac{\sigma_p}{\sigma_u} = C_2 \cdot (\rho^*)^{n_2} \qquad (6)$$

$$\varepsilon_{c,p} = 1 - \alpha \cdot \rho^* \qquad (7)$$

Some authors determined experimentally these parameters for foams[12],

honeycombs[38], some porous biomaterials[18] and AM strcutures[7]. In the case of gyroid structures, Yan et al.[43] studied Ti–6Al–4V non-graded giroid structures and determined these variables using logarithmic diagrams and determined that . Yang et al.[43] determined these parameters for graded and non-graded gyroid cellular structures made of 316L. Their studies reflected substantially different values of the parameters depending on the material so they must be determined experimentally. In this work, it has been used also the method defined by Yan et al.[43]

The densification point and elastic point shown here can be used to compare materials, as Avalle [5] pointed out by comparing and tailoring polymeric foams and combining stress–strain curves with stress–density diagrams. These works studied the capability of foam to absorb energy, using the area below the stress–strain curve (Fig. 3). For the non-graded gyroid structures that also follow the Gibson–Ashby model [43], an increase in the volume fraction implies an increase in the density and also an increase in the stress values ($\sigma_{c,e}$, $\sigma_{c,d}$), as well as the capability to absorb energy, along with lower strain at the densification point. This is due to the reduction of space inside the unit cell, which decreases the strain needed to contact different surfaces of the unit; as a result, the densification point is reached with a lower strain (reduction in $\varepsilon_{c,d}$). However, in some cases (Fig. 3), it can be observed that to absorb the same amount of energy (W_{abs}), a lower volume fraction (which also implies that the material has lower stiffness) suggests higher maximum stress because the densification point is exceeded. Moreover, if the material is excessively stiff (volume fraction is too high), higher stress appears because the stress in the plateau zone increases; furthermore, the strain reached is low, so the capability to absorb energy in the plateau zone is not sufficiently exploited. However, the stiffness could be reduced using a lower volume fraction, which would imply the same capability to absorb energy but with a lower stress level. Conversely, if

the volume fraction is excessively low, the materials are not sufficientyly stiff and have excesive deformation; they absorb the same energy and the densification point is passed. Consequently, the stress increases exponentially, implying higher stress levels toward the end. Finally, when the optimum volume fraction lies between these values, the material can absorb energy in the plateau zone.

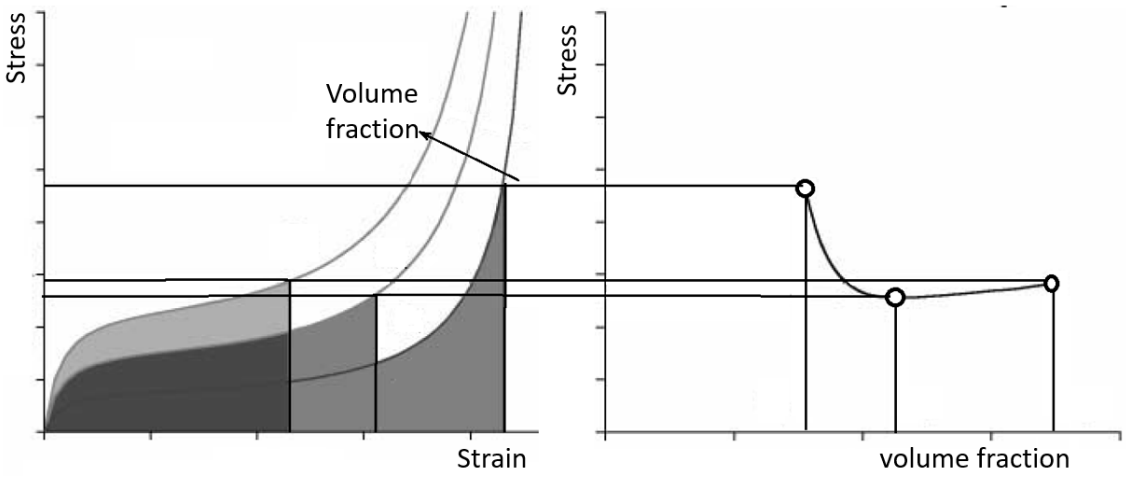

Figure 3. Influence of the volume fraction and the density in the stress–strain curve of a material at maximum stress

The absorbed-energy–stress diagrams (Fig. 4) are also useful for comparing different volume fractions and to determine the maximum stress that can be reached by the material to absorb a certain amount of energy. These curves can also be used to determine an optimal envelope curve that indicates the optimal volume fraction to absorb certain energy with the lowest stress level. In the case of polymeric foams, Avalle et al. [5] mathematically demonstrated the existence of a line with an increasing slopethat begins at the origin, which defines the optimal envelope curve. Accordingly, the optimal point for this material is close to the stress at the densification point ($\sigma_{c,d}$). These diagrams are also useful for selecting the optimum material with the lowest stress levels to absorb a certain amount of energy. The structure with the highest or lowest energy absorption in some cases may not necessarily be optimum.

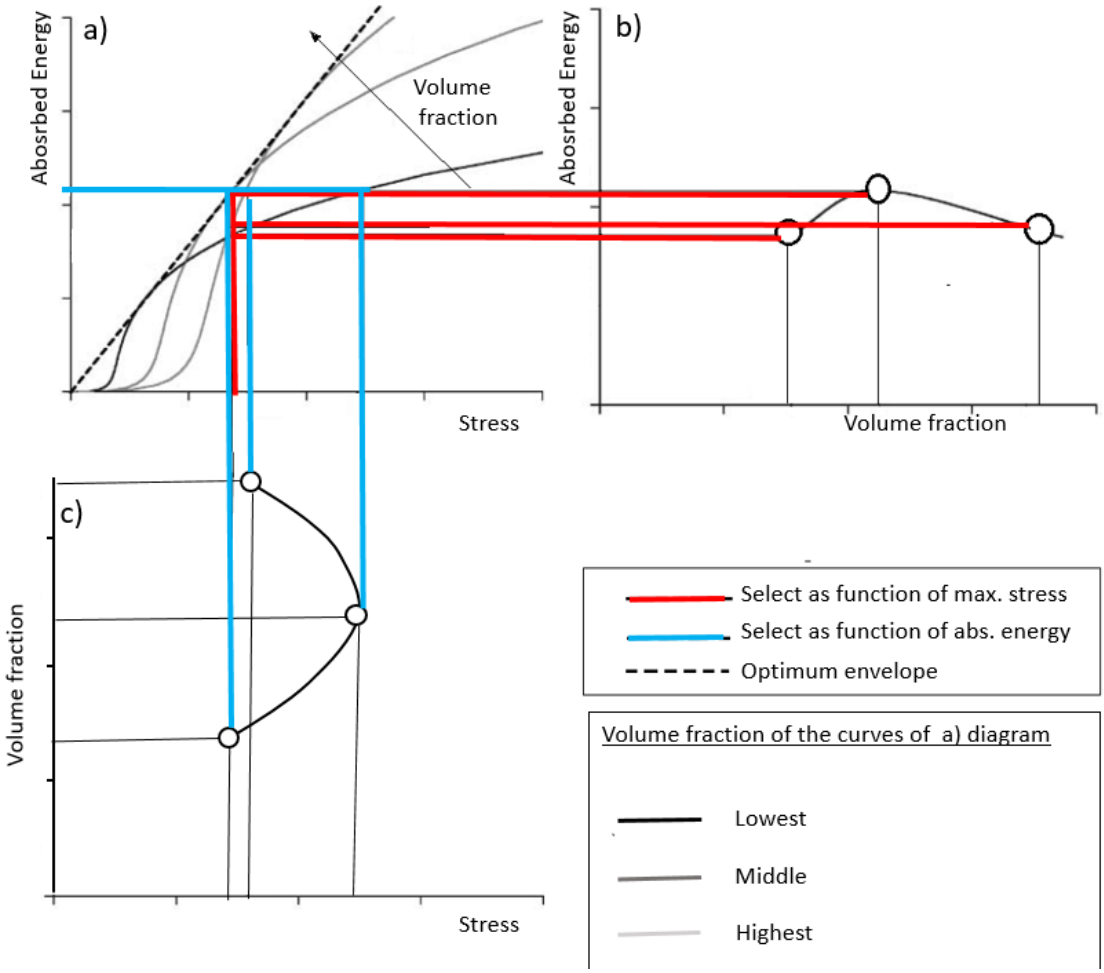

Figure 4. Influence of the volume fraction and the density on the absorbed energy and maximum stress reached.

Efficiency (*E*) is another interesting indicator proposed by Miltz and Ramon [26] and is defined as the ratio of absorbed energy to stress:

$$E = \frac{\int_o^{\varepsilon_i} \sigma d\varepsilon}{\sigma_i} \qquad (8)$$

Avalle [5] also mathematically demonstrated for polymeric foam that, for the same type of foam with different densities, the optimal efficiency is constant (Fig. 5). These diagrams can be used to select the most efficient lattice structure (optimal volume fraction value) for certain maximum stress. Iso-energy curves can also be plotted in these diagrams to select the most efficient structure configuration or the configuration with lower stress. These diagrams additionally show that, for certain stress limits

(vertical line) or a certain amount of energy absorption, the structure with the higher or lower volume fraction is not the most efficient one.

In the efficiency vs. stress diagram (Fig. 5.b), it has been plotted the curves for specimens with different increasing volume fraction; the curves shows that there is a maximum efficiency that is the same for all the specimes independently of the volume fraction, like Avalle [5] demonstrated. Additionally, the stress at the maximum efficiency point increase with the volume fraction (Fig. 5.b).

In the case that it would be desired to select a configuration to absorb a quantity of energy, iso-energy curves of Fig. 5.b. will be used and it is possible to see (blue lines) that, for certain energies, the most efficient solution would not be the specimen with the highest or the lowest volume fraction (Fig. 5.a). However, the lowest the volume fraction, the lowest the maximum level of stress (Fig. 5.d).

In the case that it would be desired to select a configuration that do nor overpass a stress level (vertical line in Fig. 5.b), it is possible to see (red lines) that, for certain stress levels, the most efficient solution would not be the specimen with the highest or the lowest volume fraction (Fig. 5.c).

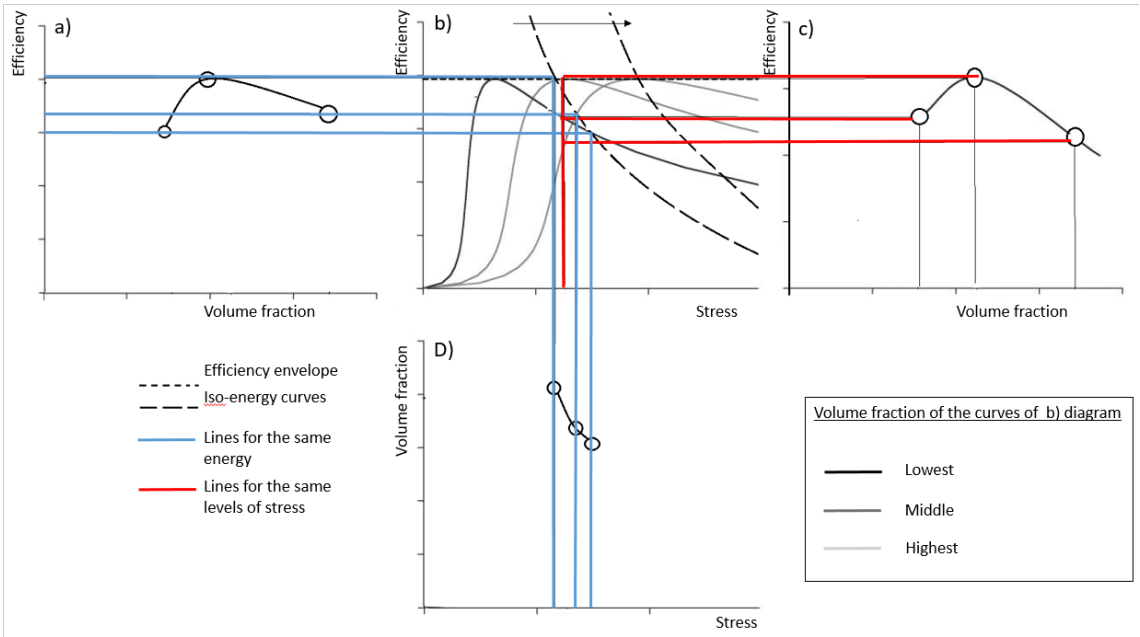

Figure 5. Influence of the volume fraction and the density on the efficiency and maximum stress reached.

However, although efficiency is useful for most common materials that follow the Gibson–Ashby model, this parameter is not adequate when the stress–strain curve does not monotonically increase because the parameter does not consider the previously reached maximum stress; consequently, the total efficiency (E_t) was proposed [16,17] to solve this drawback. This parameter is the ratio of energy to the maximum experienced stress:

$$E_t = \frac{\int_o^{\varepsilon_i} \sigma d\varepsilon}{\max\limits_{0 \le x \le \varepsilon_i} \sigma_i} \qquad (9)$$

Maskery et al. [23] further demonstrated that this indicator is useful for certain types of lattice structures.

In the same way, Miltz et al. [26] proposed another indicator, the ideality (I):

$$I = \frac{\int_o^{\varepsilon_i} \sigma d\varepsilon}{(\sigma_i \times \varepsilon_i)} \qquad (10)$$

While to calculate efficiency, only stress is considered, for ideality, both stress and strain are included to analyze how close the material is to an ideal absorber that will

be a material with constant stress across all strain ranges. The study by Miltz et al. [26] also highlighted that ideality was not an adequate indicator for materials that follow the Gibson–Ashby model because the maximum ideality appears at the beginning of the plateau zone.

Note that the abovementioned diagrams compare materials for a specific volume. However, in certain applications, such as helmet liners to reduce rotational acceleration [8], it is equally or more important to select a light material for the inner liner. Consequently, instead of using energy and stress, specific energy (W_s) and specific stress (σ_s) are more appropriate. Mathematically, it is easy to demonstrate that efficiency and ideality do not change if specific energy and specific stress are used.

In summary, specific parameters are useful for comparing materials with the same weight, and nonspecific parameters are useful for comparing different materials with the same volume.

Finally, normalized energy (W/E_{cb}) versus normalized stress (σ/E_{cb}) characteristics have been used [23,44] to compare AM structures and foam materials with materials of different origins. In this case, E_{cb} is the Young's modulus of the solid specimen of the AM materials and, in the case of foams, the Young's modulus of non-foam materials.

3. Results and discussion

The analysis of the stress–strain curve of the different materials (Fig. 6) shows that high-grade gyroid HG25% partially follows the Gibson–Ashby model because it presents an initial elastic zone with linear behavior and a final densification zone with exponential behavior. However, these configurations do not exhibit the constant plateau

of the Gibson–Ashby model. The results show that, depending on the material, the behavior in the intermediate zone changes: in the case of the TPU and PA12, a constantly increasing slope with some small fluctuations appears corresponding with the collapse of each layer of the specimen. For PLA, which is a brittle material, the stress level initially appears as a peak and later decreases and appears as a plateau that is similar to the one of the Gibson–Ashby model. For ABS, initially, there is a plateau with some oscillations and afterwards, the curve shows an increase with some oscillations. Comparing the result of the HG25% structure with the equivalent non-graded one, NG25%, the non-graded material follows the Gibson–Ashby model, as do all the studied materials. Nevertheless, for PLA, an initial peak is also observed at the beginning of the plateau. The comparison between these configurations shows that, for the PA12 and TPU, the initial level of strain after the elastic zone is lower for the non-graded structure and increases linearly to reach a higher level of stress. Additionally, the densification point appears with higher strains for the graded structure; this is especially significant in the case of the TPU material. For PLA, the densification appears with a lower strain and the stress level in the intermediate zone is smaller for the graded structure.

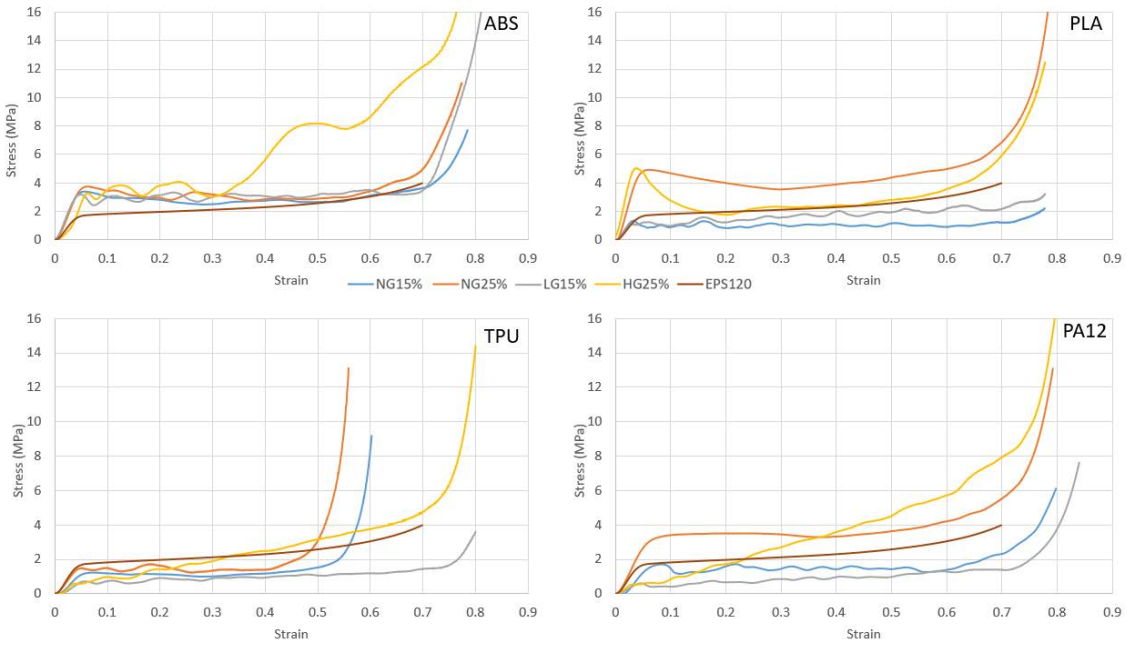

Figure 6. Stress–strain curves for the studied materials and structures.

Note that LG15% also follows the Gibson–Ashby model. In terms of the level of stress, comparing this structure with NG15%, it can be observed that, for ABS, there are no significant differences between the two structures; moreover, the densification point appears approximately at the same strain level. In the case of PLA, the level of stress is significantly higher for the graded structure, which increases slightly in the plateau zone. For TPU and PA12, while the stress beyond the elastic zone is significantly lower for the graded structure, that in the plateau is similar; the densification point appears at a much higher strain implying a higher capability to absorb energy in a controlled manner. Thus, there is no clear pattern in the stress–strain curve of the graded structures and it is essential to analyze the stress–strain curve of the original materials to establish a possible relationship. This is shown in Fig. 7.

Additionally, for ABS, the non-graded structures have a more stable stress–strain curve and densification appears with higher strains, especially in the case of HG25%. For PLA, the low-graded structures increase the stress levels in the plateau zone and generate a slightly increasing curve that enhances the overall mechanical

properties of the structure. The mechanical properties of the high-graded structures are reduced and an undesirable initial high peak is generated. In all the cases, densification appears approximately at the same strain level. While TPU shows lower mechanical properties, the graded structures delay the densification point compared with the non-graded ones. Additionally, high-graded structures generate a constantly increasing curve. Finally, PA12 presents a similar behavior to that of TPU, but there is no significant increase in the strain at the densification point. Main mechanical properties that are going to be used to determine the parameter of the equations 5 to 7 are condenser in Table 3.

Table 3. Main mechanical properties of the graded and non-graded structures

ABS	E_c **(MPa)**	σ_p **(MPa)**	$\alpha_{c,p}$	**PLA**	E_c **(MPa)**	σ_p **(MPa)**	$\alpha_{c,p}$
NG15%	78.2	2.52	0.72	NG15%	58.6	0.93	0.72
NG25%	91.1	2.89	0.68	NG25%	127.7	ND	0.66
LG15%	89.9	2.78	0.63	LG15%	59.0	3.55	0.63
NG15%	94.3	3.4	ND	NG15%	168.1	1.77	0.52
TPU	E_c **(MPa)**	σ_p **(MPa)**	$\alpha_{c,p}$	**PA12**	E_c **(MPa)**	σ_p **(MPa)**	$\alpha_{c,p}$
NG15%	27.0	0.99	0.45	NG15%	36.6	1.24	0.6
NG25%	40.3	1.34	0.41	NG25%	62.2	3.55	0.53
LG15%	21.5	0.62	0.73	LG15%	15.1	0.42	0.55
NG15%	ND	ND	0.69	NG15%	ND	ND	ND

It can be observed in this table that, with the same equivalent volume fraction, graded and non.graded strcutures exhibit different mechanical properties; additionally, in some cases the shape of the stress-strain curve of some graded materials do not follow the Gibson–Ashby model. Thus, it has been obtained the Gibson–Ashby parameters only for non-graded structures (Table 4); this table shows a huge variation in all the parameters and there is not a clear relationship of this parameters between materials. Consequently, they cannot obtained from a similar material (TPU and PLA) or with the same failure mode and they must be obtained experimentally for each

material.

Table 4 Gibson–Ashby model parameters

	C_1	C_2	n_1	n_2	α
ABS	0.087	0.00267	0.298	0.268	0.847
PLA	0.526	0.0671	1.52	2.62	0.843
TPU	5.65	0.143	0.786	0.593	0.529
PA12	0.180	0.0346	1.03	1.94	0.706

Comparison of these structures with EPS reveals that the EPS curve exhibits no oscillations that are due to the collapse of cells in AM structures. Additionally, in some cases, EPS has higher specific properties (TPU), but in other cases lower (ABS).

The specific stress–strain curves (Fig. 7), used to compare structures having the same weights, along with the curve for the original material, show that the shape of the original material conditioned the stress–strain curve, especially for the high-graded structure. The ABS solid material has an initial peak at the end of the elastic zone, followed by a constantly increasing curve that ends with an exponential behavior beginning at a relatively low strain (0.3%). This curve shape indicates the shape of the gyroid structure, which also presents an initial peak. Additionally, the exponential behavior of the original material with low strains is reflected in the behavior of the high-graded structure but does not condition the other structures. The analysis of the specific stress levels also shows that a higher volume fraction implies lower initial specific stress levels and a lower specific Young’s modulus in the elastic zone.

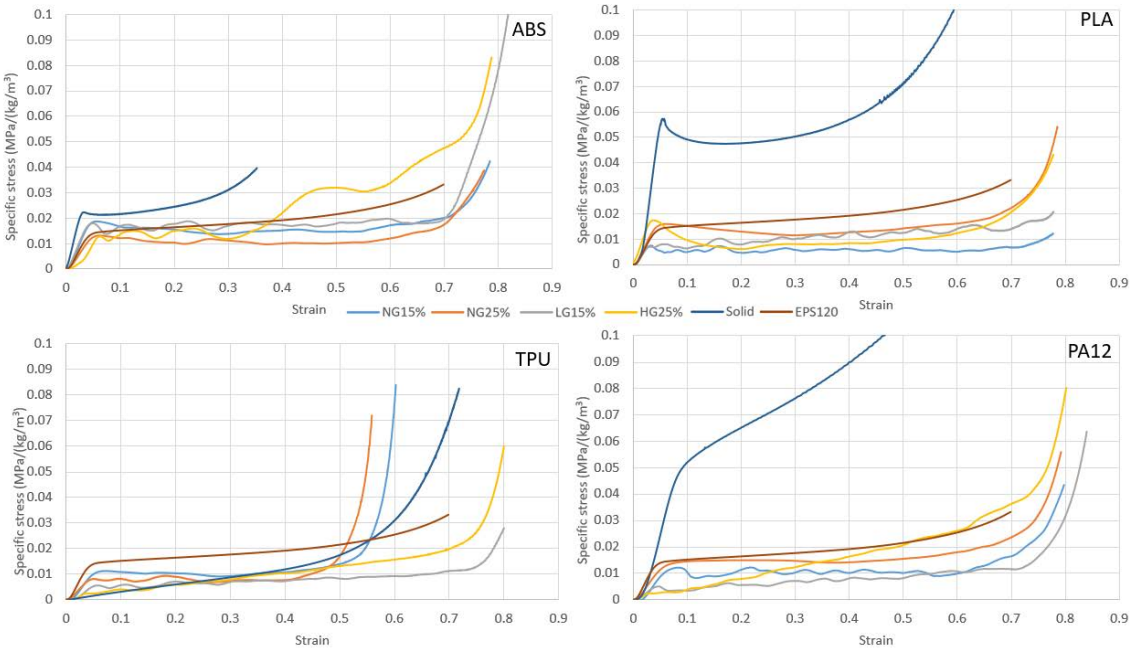

Figure 7. Specific stress–strain curve for the studied materials and structures.

In the case of PLA, while this material shows higher specific stress than that in ABS, the specific stress levels of the gyroid structures are lower; additionally, higher volume fractions imply higher specific stress levels. The PLA curve shape also shows an initial peak that is higher than that of ABS, which is reflected in the higher initial peak of the gyroid structures. For PLA, the exponential behavior of the curve appears with higher strain, thus delaying the strain at which densification occurs in the gyroid structures. Furthermore, the densification of the PLA original material, that appears with high strains, will highly influence the shape of the high-graded gyroid structure.

The TPU solid material initially exhibits a linearly increasing curve that ends with an exponential zone, while PA12 conditions a bi-linear curve that also ends with an exponential zone. This shape condition, especially the shape of both graded structures, also presents a constantly increasing shape that ends with an exponential zone. The slope of this curve increases for a higher variation of the volume fraction of the graded structure. However, in the case of the non-graded structures, the Gibson–Ashby model

is followed (Fig. 7).

The main conclusion of the analysis of the original materials is that, while they influence the curve shape of the graded structures, they do not influence the curve shape of the non-graded structures that follow the Gibson–Ashby model.

Comparison of these materials with the EPS120 shows that EPS has higher specific properties and there are no oscillations in its curve.

Fig. 8 shows the absorbed energy per unit volume of each structure. Depending on the material, either graded or non-graded structures have high energy-absorbing capabilities. In ABS, the graded structures have a higher capability to absorb energy, while in PA12, non-graded structures are superior. For PLA, while NG25% can absorb more energy than HG25%, NG15% has a lower energy-absorbing capability than LG15%. In TPU, NG25% and HG25% have approximately the same capability, while it is higher in NG15% than in LG15%.

The comparative analysis with EPS120 shows that although ABS has a higher capability to absorb energy, it is lower in TPU structures. In the case of PA12 and PLA, the high volume fraction structures have higher capabilities to absorb energy than the low volume fraction structures.

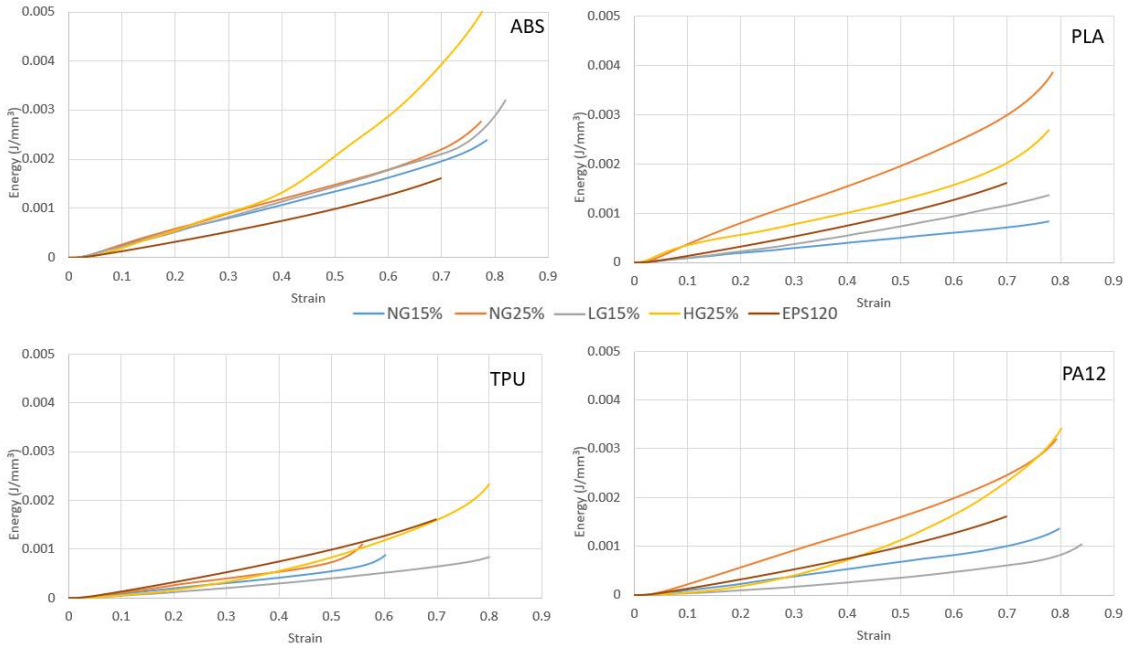

Figure 8. Energy absorbed per unit of volume vs. strain for the studied materials and structures.

In terms of energy absorbed per unit of mass (Fig. 9), it can also be observed that EPS has a higher capability to absorb energy, except for ABS, which has energy-absorbing capability similar to graded structures, qualifying it as a substitute. Compared with the solid material, it can be observed that, except for TPU, the other gyroid structures can absorb less energy per unit mass.

The analysis also indicates that, depending on the material, the structure with the highest capability to absorb energy per unit of mass differs. In the case of ABS, LG15% has the highest capability until it is surpassed by HG15%. In the case of non-graded structures, the lower the volume fraction, the higher the energy-absorbing capability. In the case of PLA, NG25% has the highest capability and, further, both graded structures have similar capabilities. Finally, NG15% had the lowest energy-absorbing capability. In the case of TPU, NG15% has the highest capability followed by NG25%. Up to a certain point, at a strain of approximately 45%, both graded structures have similar capabilities and, after this point, the high-graded structure has the highest capability.

Finally, in the case of PA12, NG25% has the highest capability followed by NG15%, until at a certain point it is surpassed by HG25%. LG15% has the lowest capability.

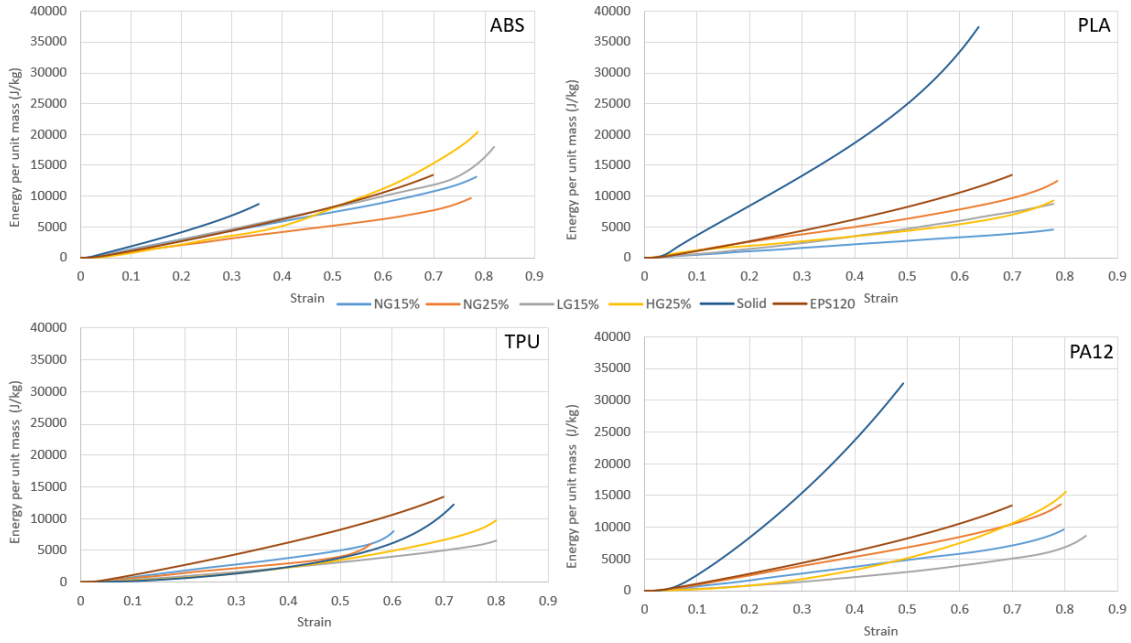

Figure 9. Energy absorbed per unit mass vs. strain for the studied materials and structures.

The analysis of the total effectivity (Fig. 10) shows that high-graded structures have the lowest effectivity among all the gyroid structures; thus, they do not efficiently use the material to absorb energy. In the low-graded structures of EPS and TPU, this configuration has the highest total efficiency; however, in TPU until a strain of 50%, the non-graded equivalent structure has higher efficiency. For the other materials, NG15% has higher efficiency than LG15%; thus, LG15% superior only in certain cases. The efficiency of the graded structures for the TPU appears at a higher strain, owing to the delay in densification. Compared with the original materials, gyroid structures increase the efficiency in all the cases except for the high-graded PA12 structure. Comparing the gyroid structures with EPS reveals that it is possible to obtain a configuration with higher efficiency for all the materials. Nevertheless, some configurations also have lower efficiency.

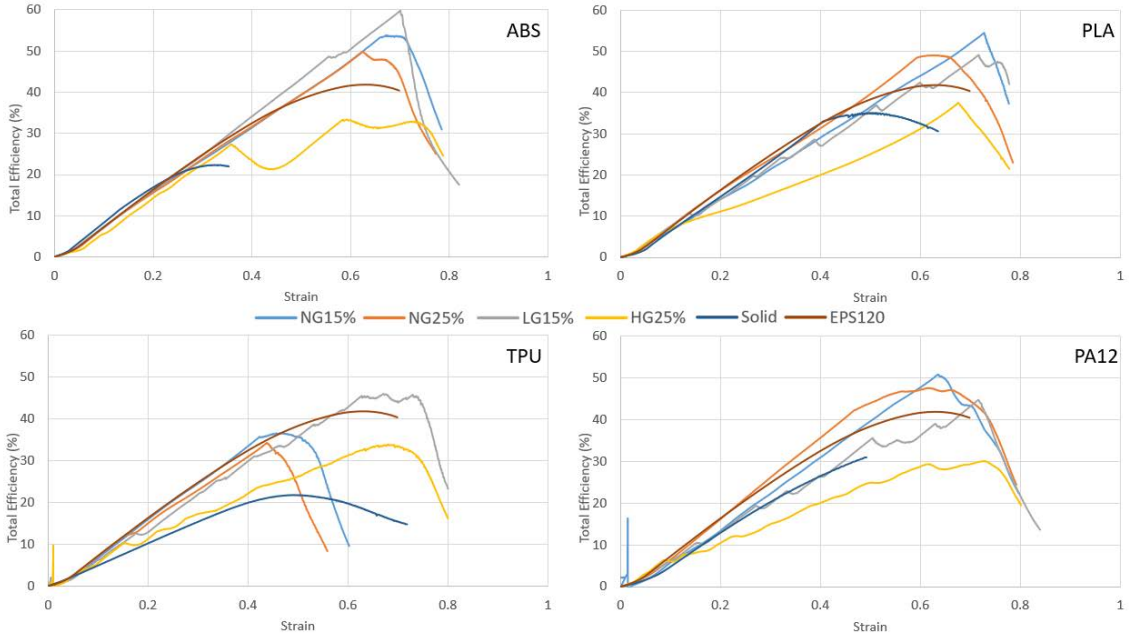

Figure 10. Total efficiency vs. strain for the studied materials and structures.

The graphs of the total efficiency vs. stress (Fig. 11) also illustrate the stress level at which maximum efficiency appears. While the high-graded structure has the lowest maximum total efficiency, the range of stress with significant efficiency is higher than that of other materials. For some materials (TPU and ABS), the maximum efficiency appears approximately at the same stress levels, whereas in the case of PLA and PA12, this does not occur.

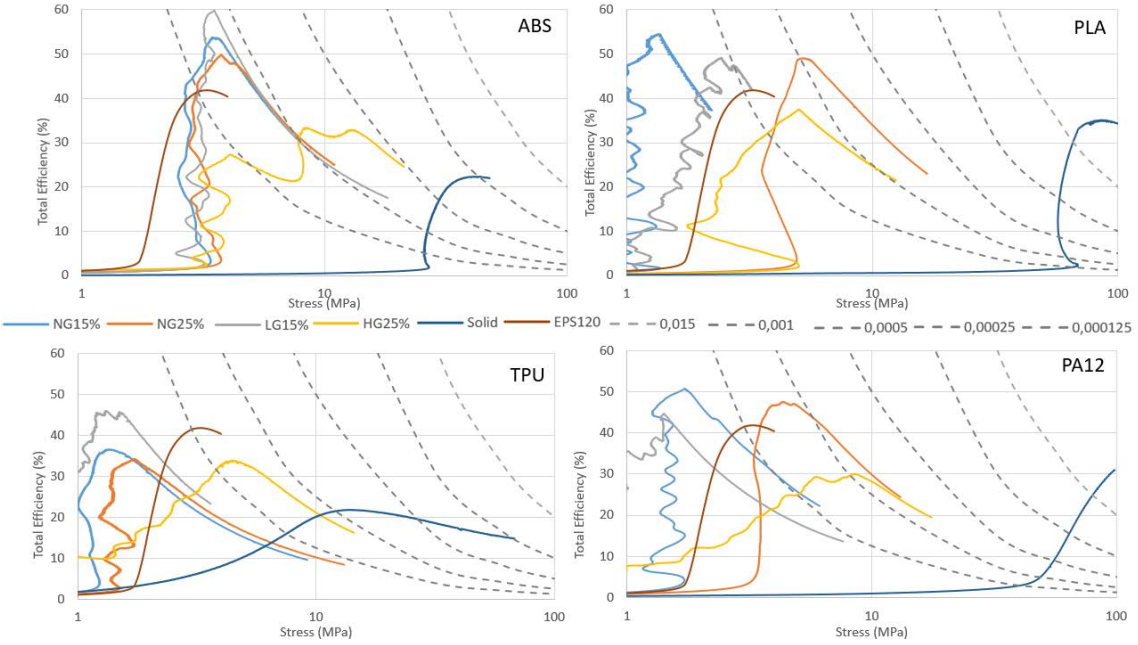

Figure 11. Total efficiency vs. stress for the studied materials and structures. Grey lines: iso-energy curves in J/kg.

The analysis of ideality (Fig. 12) indicates that in all cases, except for PLA and the high-graded structure, non-graded structures have higher ideality for the entire or major part of the strain range. The non-graded structures have a higher ideality than EPS, but the ideality of the gyroid structures has some oscillations due to the layer-to-layer collapse. This phenomenon also appeared in the previous graphs for total efficiency. It is important to note that gyroid structures, in most cases, generate more ideal materials than solid materials do.

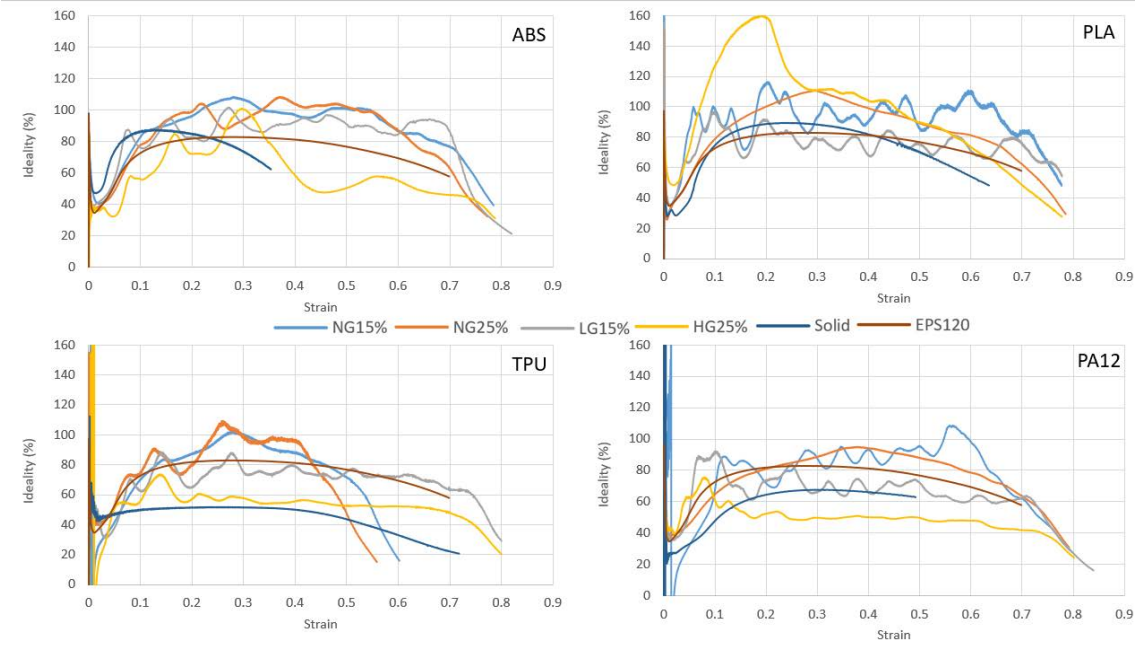

Figure 12. Ideality vs. strain for the studied materials and structures.

Fig. 13 shows plots of normalized energy vs. normalized stress; in most cases, the non-graded structure has higher normalized energy than the graded structures, except for ABS, which has approximately the same normalized energy for all the structures and most of the strain range. Particularly, the gyroid structures appear to have lower normalized energy than the solid material and EPS, except in the case of the TPU. Hence, at the same maximum stress level, the original materials and EPS can absorb more energy than the gyroid structures; furthermore, the non-graded structures have

higher capabilities to absorb energy at the same stress, in most cases.

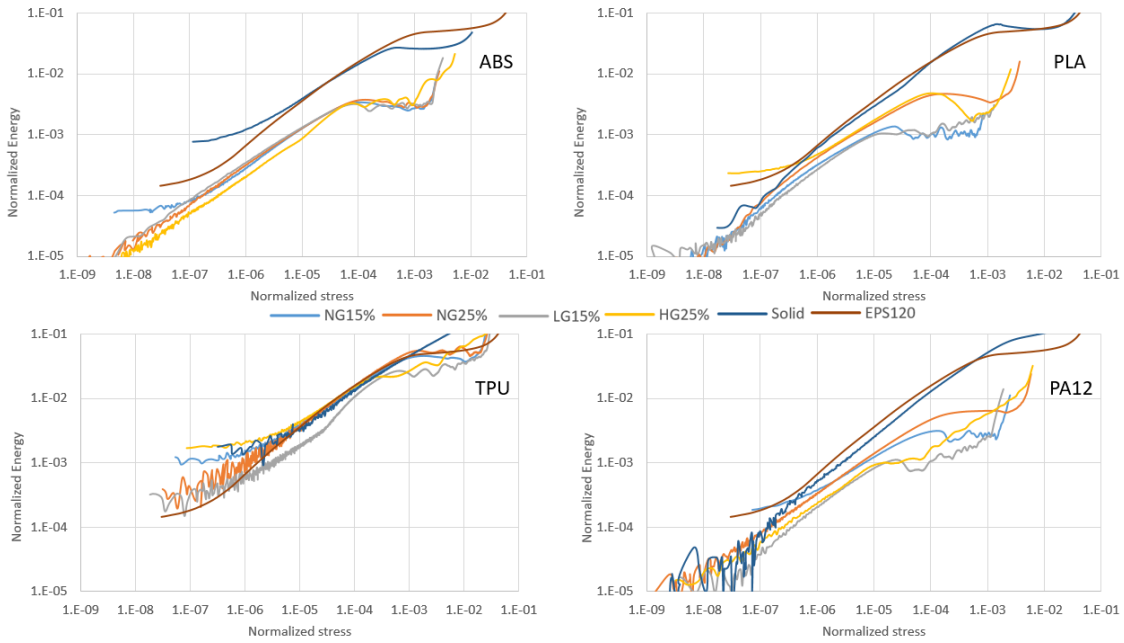

Figure 13. Normalized energy vs. normalized stress for the studied materials and structures.

Finally, Fig. 14 illustrates some compression tests for different materials and configurations. In all the studies, for both the graded and non-graded structures, the structures were seen to collapse layer-by-layer, with no other type of collapse present in the investigated materials. Furthermore, while ABS and PLA cannot recover their initial shapes and present a high permanent deformation after the test, TPU completely recovers its initial shape and can thus absorb other impacts; therefore, TPU can be a suitable material in the case of multiple impacts. As for PA12, the material partially recovers its initial shape but exhibits permanent deformation.

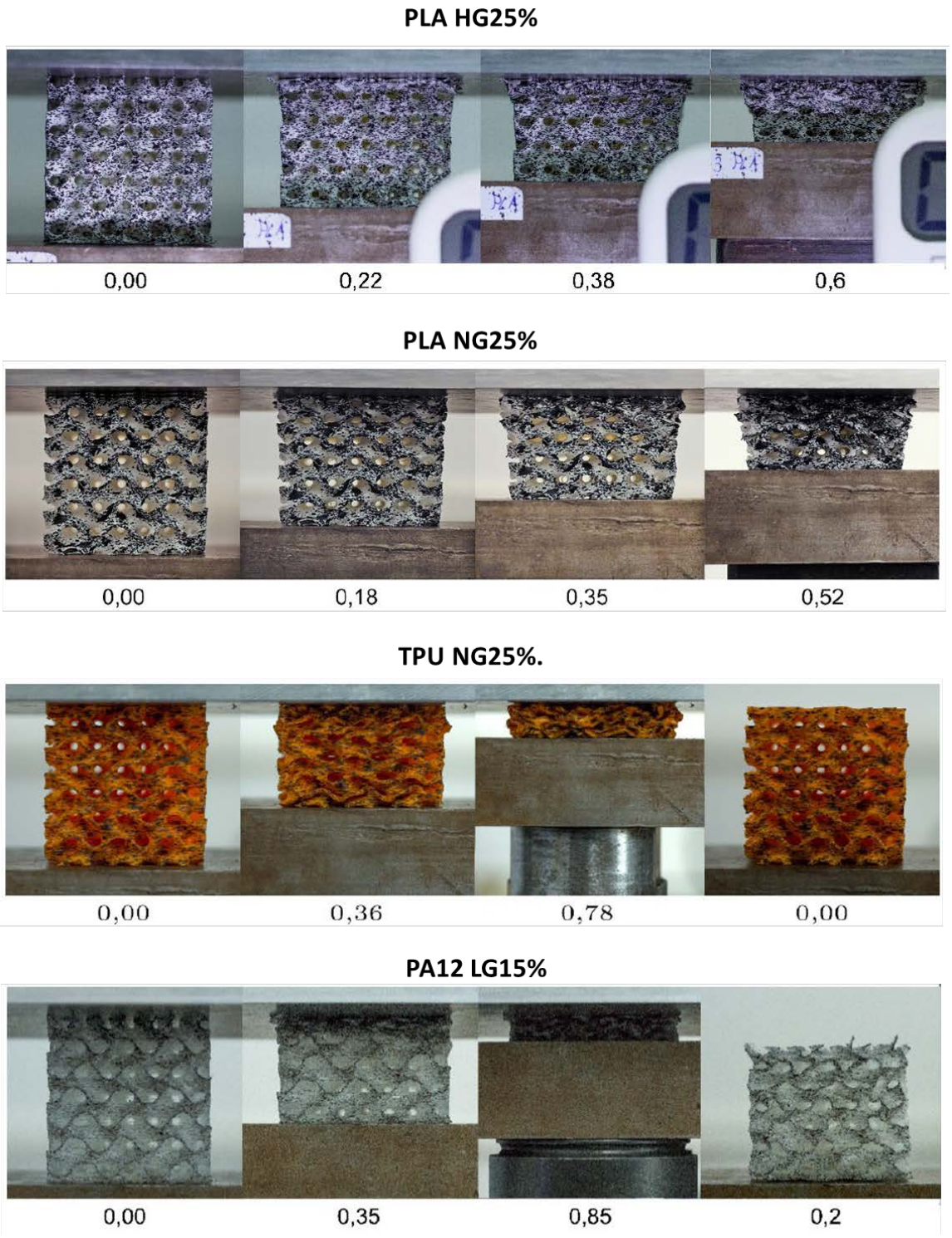

Figure 14. Images demonstrating the compression testing of some materials and structures. In the botton of each image appear the strain.

4. Conclusion

In this study, we examined the mechanical properties and energy absorption capabilities under quasi-static compression of non-graded and graded gyroid structures

manufactured using fused filament fabrication for various thermoplastic materials. While the shape of the stress–strain curves for graded studied structures is highly influenced by the original material, for non-graded structures, this influence is not so significant and most studied models follow the Gibson–Ashby material model. For a graded structure, an increasing curve is observed in the area between the elastic zone and the densification zone that could be typically approximated with a linear curve. This curve has a higher slope in the high-graded structure than in the low-graded structure. Additionally, for TPU, the densification appears with significantly higher strains for the graded structures. Hence, for this material, the significant zone of the curve is extended. For PA12, the same phenomenon occurs, but the increase is not very high. In relationship with the parameters of the Gibson–Ashby material model, it has not been obtained a relationship that can be used to determine any of these parameters without experimental test of the studied material.

The comparative analysis with EPS120, reveals that with these configurations, it is possible to obtain a material with similar or superior mechanical specific and nonspecific properties; hence, the capability of absorbing energy per unit volume and per unit mass is also similar or higher. Additionally, for some materials, the densification appears at a higher strain level using gyroid structures allowing the material to deform significantly before reaching the densification zone, which implies an exponential behavior of the stiffness. In the case of TPU, the lower initial mechanical properties imply a lower capability to absorb energy per unit volume; however, in the case of other materials that have a higher capability to absorb energy per unit volume, the higher density (between 20 and 150% higher) penalizes the capability to absorb energy per unit mass. Additionally, it must also be noted that the internal collapse of the cells of the gyroid structures generates some oscillations in the stress–strain curves of

the material.

Comparative analysis of the graded and non-graded structures shows that in some cases (ABS and PLA), graded structures exhibit higher capabilities to absorb energy than equivalent non-graded ones, but in other cases (PLA and PA12), non-graded structures absorb more energy. Additionally, TPU can recover its initial shape completely, while PA12 can recover partially. Subsequent compression tests have not been carried out to analyze resilience, to determine if these materials can absorb multiple loads, or to discover if they have the internal resistant structure intact.

Note that while other authors have noticed other additional collapse failure mechanisms, only a layer-by-layer collapse, which is desirable, was observed in this study.

Analysis of the total efficiency and the total ideality shows that some of the gyroid structures have higher values than the EPS and the original materials, but the curves also present some oscillations. Additionally, the results reveal that in most cases, the non-graded structures have higher efficiency and ideality; therefore, they can be utilized to absorb energy, except for the case of TPU, where although the maximum total efficiency and ideality are lower, the range of the strain with higher values is larger.

Interestingly, none of the observed patterns indicates that graded structures are superior to non-graded structures or vice versa; this behavior depends on the individual material.

Finally, it was observed that graded structures exhibit a constantly increasing stiffness in the intermediate zone of the stress–strain curve. This could imply that these

structures could generate superior energy-absorbing materials because an initial peak typically appears, during an impact, in the deceleration curve that is related to the initial stiffness of the stress–strain curve in the intermediate zone, and afterwards, the deceleration decreases. The use of graded structures that initially have lower stiffness could imply lower initial peak deceleration. However, additional studies using drop towers are essential.

Furthermore, while impacts are dynamic-load cases, this study has been focused on quasi-static compression tests; hence, additional tests that involve the influence of strain rate should be carried out.

5. Acknowledgements

The authors disclose receipt of the following financial support for the research, authorship, and/or publication of this article: This work was supported by the "University of ZaragozaCentro Universitario de la Defensa" joint Research Grant. (grant number UZCUD2019-TEC-04).

The authors would like to thank nTopology that provided the software that was essential to prepare all the CAD models.

6. References

1. Al-Ketan O, Adel Assad M, Abu Al-Rub RK. Mechanical properties of periodic interpenetrating phase composites with novel architected microstructures. Composite Structures. 2017;176:9–19. doi:10.1016/j.compstruct.2017.05.026

2. Al-Ketan O, Rowshan R, Abu Al-Rub RK. Topology-mechanical property relationship of 3D printed strut, skeletal, and sheet based periodic metallic cellular materials. Additive Manufacturing. 2018;19:167–183. doi:10.1016/j.addma.2017.12.006

3. Al-Saedi DSJ, Masood SH, Faizan-Ur-Rab M, Alomarah A, Ponnusamy P. Mechanical properties and energy absorption capability of functionally graded F2BCC lattice fabricated by SLM. Materials & Design. 2018;144:32–44. doi:10.1016/j.matdes.2018.01.059

4. Aremu A.O., Maskery I, Tuck C. A comparative finite element study of cubic unit cells for selective laser melting - Self-supporting Unit cells. :1238–1249.

5. Avalle M, Belingardi G, Montanini R. Characterization of polymeric structural foams under compressive impact loading by means of energy-absorption diagram. International Journal of Impact Engineering. 2001;25(5):455–472. doi:10.1016/S0734-743X(00)00060-9

6. van Baar GJC, Ruslin M, van Eijnatten M, Sándor GK, Forouzanfar T, Wolff J. 3D assessment of damaged bicycle helmets and corresponding craniomaxillo-mandibular skull injuries: A feasibility study. Injury. 2017;48(12):2872–2878. doi:10.1016/j.injury.2017.09.031

7. Benedetti M, Klarin J, Johansson F, Fontanari V, Luchin V, Zappini G, Molinari A. Study of the Compression Behaviour of Ti6Al4V Trabecular Structures Produced by Additive Laser Manufacturing. Materials. 2019;12(9):1471. doi:10.3390/ma12091471

8. Bliven E, Rouhier A, Tsai S, Willinger R, Bourdet N, Deck C, Madey SM, Bottlang M. Evaluation of a novel bicycle helmet concept in oblique impact testing. Accident Analysis & Prevention. 2019;124:58–65. doi:10.1016/j.aap.2018.12.017

9. Bobbert FSL, Lietaert K, Eftekhari AA, Pouran B, Ahmadi SM, Weinans H, Zadpoor AA. Additively manufactured metallic porous biomaterials based on minimal surfaces: A unique combination of topological, mechanical, and mass transport properties. Acta Biomaterialia. 2017;53:572–584. doi:10.1016/j.actbio.2017.02.024

10. Chen Z, Xie YM, Wu X, Wang Z, Li Q, Zhou S. On hybrid cellular materials based on triply periodic minimal surfaces with extreme mechanical properties. Materials and Design. 2019;183:108109. doi:10.1016/j.matdes.2019.108109

11. Depreitere B, Van Lierde C, Maene S, Plets C, Sloten J Vander, Van Audekercke R, Van der Perre G, Goffin J. Bicycle-related head injury: A study of 86 cases. Accident Analysis and Prevention. 2004;36(4):561–567. doi:10.1016/S0001-4575(03)00062-9

12. Deshpande VS, Ashby MF, Fleck NA. Foam topology: bending versus stretching dominated architectures. Acta Materialia. 2001;49(6):1035–1040. doi:10.1016/S1359-6454(00)00379-7

13. Finnoff JT, Laskowski ER, Altman KL, Diehl NN. Barriers to bicycle helmet use. Pediatrics. 2001;108(1):2–10. doi:10.1542/peds.108.1.e4

14. Ford M, Matic P, Leung A. Expanding Helmet Design Methodologies Through Brain Functional Area Representative Threat Models. In: Volume 3A: Biomedical and Biotechnology Engineering. San Diego, California, USA: American Society of Mechanical Engineers; 2013 [accessed 2020 Dec 23]. p. V03AT03A014. https://asmedigitalcollection.asme.org/IMECE/proceedings/IMECE2013/56215/San%20Diego,%20California,%20USA/261074. doi:10.1115/IMECE2013-64959

15. Gibson LJ, Ashby MF. Cellular solids: structure and properties. Cambridge university press; 1999.

16. Hanssen AG, Langseth M, Hopperstad OS. Static and dynamic crushing of square aluminium extrusions with aluminium foam filler. International Journal of Impact Engineering. 2000;24(4):347–383. doi:10.1016/S0734-743X(99)00169-4

17. Hanssen AG, Langseth M, Hopperstad OS. Static crushing of square aluminium extrusions with aluminium foam filler. International Journal of Mechanical Sciences. 1999;41(8):967–993. doi:10.1016/S0020-7403(98)00064-2

18. Kadkhodapour J, Montazerian H, Darabi ACh, Anaraki AP, Ahmadi SM, Zadpoor AA, Schmauder S. Failure mechanisms of additively manufactured porous biomaterials: Effects of porosity and type of unit cell. Journal of the Mechanical Behavior of Biomedical Materials. 2015;50:180–191. doi:10.1016/j.jmbbm.2015.06.012

19. Kapfer SC, Hyde ST, Mecke K, Arns CH, Schröder-Turk GE. Minimal surface scaffold designs for tissue engineering. Biomaterials. 2011;32(29):6875–6882. doi:10.1016/j.biomaterials.2011.06.012

20. Kladovasilakis N, Tsongas K, Tzetzis D. Finite Element Analysis of Orthopedic Hip Implant with Functionally Graded Bioinspired Lattice Structures. Biomimetics. 2020;5(3):44. doi:10.3390/biomimetics5030044

21. Li D, Liao W, Dai N, Xie YM. Comparison of mechanical properties and energy absorption of sheet-based and strut-based gyroid cellular structures with graded densities. Materials. 2019;12(13). doi:10.3390/ma12132183

22. Li Y, Feng Z, Hao L, Huang L, Xin C, Wang Y, Bilotti E, Essa K, Zhang H, Li Z, et al. A Review on Functionally Graded Materials and Structures via Additive Manufacturing: From Multi-Scale Design to Versatile Functional Properties. Advanced Materials Technologies. 2020;5(6):1900981. doi:10.1002/admt.201900981

23. Maskery I, Aboulkhair NT, Aremu AO, Tuck CJ, Ashcroft IA. Compressive failure modes and energy absorption in additively manufactured double gyroid lattices. Additive Manufacturing. 2017;16:24–29. doi:10.1016/j.addma.2017.04.003

24. Maskery I, Aboulkhair NT, Aremu AO, Tuck CJ, Ashcroft IA, Wildman RD, Hague RJM. A mechanical property evaluation of graded density Al-Si10-Mg lattice structures manufactured by selective laser melting. Materials Science and Engineering A. 2016;670:264–274. doi:10.1016/j.msea.2016.06.013

25. Mazur M, Leary M, Sun S, Vcelka M, Shidid D, Brandt M. Deformation and failure behaviour of Ti-6Al-4V lattice structures manufactured by selective laser melting (SLM). International Journal of Advanced Manufacturing Technology. 2016;84(5–8):1391–1411. doi:10.1007/s00170-015-7655-4

26. Miltz J, Ramon O. Energy absorption characteristics of polymeric foams used as cushioning materials. Polymer Engineering and Science. 1990;30(2):129–133. doi:10.1002/pen.760300210

27. Miralbes R, Ranz D, Ivens J, Gomez JA. Characterization of cork and cork agglomerates under compressive loads by means of energy absorption diagrams. European Journal of Wood and Wood Products. 2020 Nov 17 [accessed 2020 Dec 24].

http://link.springer.com/10.1007/s00107-020-01625-7. doi:10.1007/s00107-020-01625-7

28. Miralbes R, Ranz D, Pascual FJ, Zouzias D, Maza M. Characterization of additively manufactured triply periodic minimal surface structures under compressive loading. Mechanics of Advanced Materials and Structures. 2020 Nov 5:1–15. doi:10.1080/15376494.2020.1842948

29. Qasim SSB, Zafar MS, Niazi FH, Alshahwan M, Omar H, Daood U. Functionally graded biomimetic biomaterials in dentistry: an evidence-based update. Journal of Biomaterials Science, Polymer Edition. 2020;31(9):1144–1162. doi:10.1080/09205063.2020.1744289

30. Scherer MRJ. Double-Gyroid-Structured Functional Materials: Synthesis and Applications. 1st ed. 2013. Cham: Springer International Publishing : Imprint: Springer; 2013. (Springer Theses, Recognizing Outstanding Ph.D. Research). doi:10.1007/978-3-319-00354-2

31. Schoen AH. Infinite periodic minimal surfaces without self-intersections, NASA Techn. Rep. D-5541. 1970.

32. Schwarz HA. Gesammelte mathematische abhandlungen. American Mathematical Soc.; 1972.

33. Shoen A. Infinite periodic minimal surfaces without self-intersection. 1970.

34. Singh G, Pandey PM. Uniform and graded copper open cell ordered foams fabricated by rapid manufacturing: surface morphology, mechanical properties and energy absorption capacity. Materials Science and Engineering: A. 2019;761:138035. doi:10.1016/j.msea.2019.138035

35. Smith M, Guan Z, Cantwell WJ. Finite element modelling of the compressive response of lattice structures manufactured using the selective laser melting technique. International Journal of Mechanical Sciences. 2013;67:28–41. doi:10.1016/j.ijmecsci.2012.12.004

36. Speirs M, Van Hooreweder B, Van Humbeeck J, Kruth JP. Fatigue behaviour of NiTi shape memory alloy scaffolds produced by SLM, a unit cell design comparison. Journal of the Mechanical Behavior of Biomedical Materials. 2017;70:53–59. doi:10.1016/j.jmbbm.2017.01.016

37. Texto completo. [accessed 2020 Dec 9]. https://www.mdpi.com/1996-1944/12/13/2183/pdf

38. Wang A-J, McDowell DL. In-Plane Stiffness and Yield Strength of Periodic Metal Honeycombs. Journal of Engineering Materials and Technology. 2004;126(2):137–156. doi:10.1115/1.1646165

39. Xu S, Shen J, Zhou S, Huang X, Xie YM. Design of lattice structures with controlled anisotropy. Materials & Design. 2016;93:443–447. doi:10.1016/j.matdes.2016.01.007

40. Yan C, Hao L, Hussein A, Raymont D. Evaluations of cellular lattice structures manufactured using selective laser melting. International Journal of Machine Tools and Manufacture. 2012;62:32–38. doi:10.1016/j.ijmachtools.2012.06.002

41. Yan C, Hao L, Hussein A, Young P. Ti-6Al-4V triply periodic minimal surface structures for bone implants fabricated via selective laser melting. Journal of the Mechanical Behavior of Biomedical Materials. 2015;51:61–73. doi:10.1016/j.jmbbm.2015.06.024

42. Yan C, Hao L, Hussein A, Young P, Raymont D. Advanced lightweight 316L stainless steel cellular lattice structures fabricated via selective laser melting. Materials and Design. 2014;55:533–541. doi:10.1016/j.matdes.2013.10.027

43. Yang L, Mertens R, Ferrucci M, Yan C, Shi Y, Yang S. Continuous graded Gyroid cellular structures fabricated by selective laser melting: Design, manufacturing and mechanical properties. Materials & Design. 2019;162:394–404. doi:10.1016/j.matdes.2018.12.007

44. Yu S, Sun J, Bai J. Investigation of functionally graded TPMS structures fabricated by additive manufacturing. Materials & Design. 2019;182:108021. doi:10.1016/j.matdes.2019.108021

45. Zhang L, Feih S, Daynes S, Chang S, Wang MY, Wei J, Lu WF. Energy absorption characteristics of metallic triply periodic minimal surface sheet structures under compressive loading. Additive Manufacturing. 2018;23:505–515. doi:10.1016/j.addma.2018.08.007